Electron Binding Capabilities of Some Silylenes Having Small Singlet−Triplet Splittings or Triplet Ground States

ARTICLE *in* THE JOURNAL OF PHYSICAL CHEMISTRY A · FEBRUARY 2007

Impact Factor: 2.69 · DOI: 10.1021/jp066551e · Source: PubMed

3 AUTHORS, INCLUDING:

Piotr Skurski
University of Gdansk
140 PUBLICATIONS **3,378** CITATIONS

SEE PROFILE

Electron Binding Capabilities of Some Silylenes Having Small Singlet−Triplet Splittings or Triplet Ground States

Josef Kalcher,*,† Piotr Skurski,‡ and Jack Simons

Department of Chemistry, Henry Eyring Center for Theoretical Chemistry, University of Utah, Salt Lake City, Utah 84112

Received: October 5, 2006; In Final Form: November 15, 2006

Several silyl and alkaline metal substituted silylenes have been investigated using the CAS-ACPF method in conjunction with the aug-cc-pVTZ basis sets. Silylsilylene and disilylsilylene are found to have singlet ground states with ΔE_{ST} values of 0.676 and 0.319 eV, respectively. The adiabatic ground state electron affinities are found to be 1.572 and 2.361 eV for $HSiSiH_3$ and $Si(SiH_3)_2$. respectively. Both silylenes possesses a stable $^2A_1$ excited negative ion state, with respective adiabatic EA values of 0.037 and 1.000 eV. In contrast, all silylenes with at least one akaline metal substituent exhibit triplet neutral ground states. The metalated silylenes HSiLi, HSiNa, $LiSiSiH_3$, NaSiLi, $SiLi_2$, and $SiNa_2$ have adiabatic ground state EAs somewhat below 1 eV, but each of these negatively charged system possesses up to three bound excited negative ion states, some of which are dipole-bound states.

I. Introduction

Silylenes have attracted much attention over the years due to their importance as transient species[1,2] in the course of photochemical as well as thermal reactions of silanes. Moreover, the high versatility of silylenes underlines their great utility in research.[3] In addition the conundrum of different ground state multiplicities of silylene, which owns a singlet ground state while its lighter congener, methylene, has a triplet ground state, has fostered many investigations to find a rationale for the preference of different ground state multiplicities in the lightest and the second lightest group 14 dihydrides. In a series of seminal investigations, the group of Harrison[4−8] has laid out the basic structure of singlet−triplet splittings in carbenes and by analogy in silylenes. These researchers have been the first to point out that lithium substituents would lead to triplet electronic ground states in silylenes.

A recent CASSCF energy partitioning study by Apeloig et al.[9] has revealed that no more than 60% of the observed singlet−triplet energy difference of some 29 kcal/mol between $^3CH_2$ and $^1SiH_2$ can be attributed to energy contributions from the highest-lying valence electrons. The search for triplet ground state silylenes has been inspired by theoretical studies of Gordon[10] on the bending potential energy curves for $^1SiH_2$ and $^3SiH_2$, which revealed that the triplet state is the lowest neutral electronic state for bond angles $\geq 125°$. The fact that the triplet state has a larger equilibrium bond angle than the singlet state can be qualitatively argued following Gaspar et al.[11] For a bond angle of 180° (i.e., linear SiH_2), the valence electron configuration is π_u^2 which correponds to a triplet ground state. Upon bending, the degeneracy of the π_u orbitals is lifted. Although the component orthogonal to the molecular plane retains its π character, the in-plane component acquires more and more σ character and evolves into a σ-type orbital as the bonding angle gets smaller and smaller. Moreover, the energy gap between the Si π and σ orbitals grows as the angle decreases. Consequently, for small bond angles, both electrons reside in the σ-type orbital, which leads to the singlet ground state and the excitation energy to the triplet state, formally by promoting one of the σ-type HOMO electrons to the π-type LUMO, is rather high.

From this analysis, it is clear that the triplet state can be favored over the singlet state by causing the σ-type and the π-type orbitals to be spatially and energetically similar. This similarity can be achieved in two different ways: (1) a simple strategy is the use of bulky substituents,[11−14] so that a large bond angle results for steric reasons. This thread of research culminated in the success of Sekiguchi et al.[15] in identifying bis(tri-*tert*-butylsilyl)silylene to have a triplet ground state. (2) Earlier theoretical investigations by Colvin et al.[16] have revealed that highly electropositive substituents such as Li also reduce the s-admixture of the σ-type orbital, thus raising its energy closer to that of the π-type orbital and favoring triplet ground states. The propensity for high-spin ground states in diatomics containing alkaline metal atoms has also be noted previously by Boldyrev and Simons.[17−19] A less pronounced but similar effect has been found by Grev et al.[20] for the silyl-substituent.

Despite this plethora of theoretical as well as experimental investigations on triplet ground state silylenes, there are few investigations on the electron affinities of silylenes.[1,21−29] Theoretical studies on methyl- and halogen-substituted silylenes have appeared[28,29] showing that these species possess neutral singlet ground states and that the corresponding negative ions have only one bound state. A theoretical study by Kalcher[30] on cyanosilylene anions has shown that there exist excited anion states, but they represent dipole-bound rather than valence-bound excited negative ion states. To our knowledge, there is no systematic investigation of the electron binding capabilities of silylenes with small singlet−triplet gaps or with triplet ground states. In many spectroscopic investigations, however, negative

* To whom correspondence should be addressed. E-mail: josef.kalcher@uni-graz.at.

† Permanent address: Karl-Franzens-University Graz, Institute for Chemistry (Theoretical Chemistry), Strassoldogasse 10, A-8010 Graz, Austria.

‡ Permanent address: Department of Chemistry, University of Gdańsk, Sobieskiego 18, 80-952 Gdańsk, Poland.

10.1021/jp066551e CCC: $37.00
Published on Web 12/22/2006

SCHEME 1: Sketch of the Highest-Lying Molecular Orbitals Involved in the Singlet ($\sigma^2\pi^0$) and Triplet ($\sigma^1\pi^1$) Neutral States and the Negative Ion Ground States ($\sigma^2\pi^1$) of the Investigated Silylenes

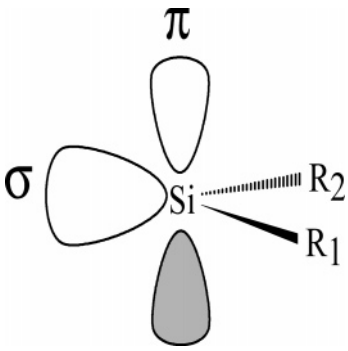

ions are used as precursors and the neutral states are studied via photodetachment spectroscopy. Depending on their production history,[31] some anions can exist in higher excited or in unexpected spin states.[32,33] It is, therefore, of vital interest to have also at least some information on the anion states of the corresponding silylenes.

The present investigation is devoted to the exploration of bound negative ion states in silylenes with silyl-substituents and lithium and sodium substituted silylenes. A special focus is given to the question whether or not there exist excited negative ion states.

II. Methodological Approach

The basis sets employed for this study are the augmented correlation consistent valence triple-ζ aug-cc-pVTZ (AVTZ) contracted sets of Dunning[34] and Woon and Dunning.[35] The reference wavefunctions for all electronic states have been computed at the full-valence complete active space (CAS) level of theory,[36] except for SiH_3-substituted species, where only the CAS(2,2) ansatz has been employed for the neutral and CAS(3,2) for the negatively charged species. These correspond essentially to RHF reference wavefunctions, except for the singlet electronic states. These reference wavefunctions have been chosen for the largest investigated systems, since a full-valence CAS expansion would yield an untractable number of configuration state functions (CSF) in the subsequent CAS-averaged coupled pair functional[37] (CAS-ACPF)-expansion, as a result of which any geometry optimizations would have been thwarted. All of these reference wavefunctions have been combined with the ACPF-method to evaluate the dynamical electron correlation. This approach will be abbreviated in the following by the acronym CAS(2,2)-ACPF in the case of CAS(2,2) reference wavefunctions, like in the treatment of the electronic states of the neutral species $HSiSiH_3$, $Si(SiH_3)_2$, and $LiSiSiH_3$, and CAS(3,2)-ACPF for their negatively charged electronic states, where CAS(3,2) reference wavefunctions have been employed. Scheme 1 shows the highest-lying MOs involved in determining the symmetries of the energetically most favorable neutral singlet ($\cdots\sigma^2\pi^0$) or triplet ($\cdots\sigma^1\pi^1$) states and the negative ion ground states ($\cdots\sigma^2\pi^1$). From this orbital sketch, it becomes clear that within this (σ,π) orbital space CAS(2,2) wavefunctions and CAS(3,2) wavefunctions are qualitatively correct for the electronic states of the neutral silylenes and that of the negative ions, respectively, especially if these silicon-centered orbitals do not significantly interact with any of the two substituents R_1 and R_2 and can, therefore, be used as reference wavefunctions for these electronic states in high level calculations to assess the dynamical electron correlation. For all other cases, where full-valence CAS reference wavefunctions have been used, we use the acronym CAS-ACPF. We would like to emphasize that all results like geometry data, singlet−triplet splittings, and electron affinities reported and discussed in the present work refer to CAS-ACPF values if not explicitly stated otherwise. Only the valence electron correlations have been taken into account in these procedures, meaning that the Si 1s, 2s, and 2p; Li 1s; and Na 1s, 2s, and 2p electrons have not been included. The CAS-ACPF approach has been chosen for the computation of the correlation energy since this approach can be used not only for single-determinant reference wavefunctions such as Hartree−Fock but also for multiconfiguration SCF reference wavefunctions, and because it is almost perfectly size extensive. This latter property is highly desirable since it guarantees that our evaluated electron affinities are at least not biased by size extensivity errors. The adiabatic electron affinities, EA, are defined as

$$\mathrm{EA} = E_{\mathrm{neutral}}(r_0) - E_{\mathrm{anion}}(r_-)$$

where r_0 and r_- refer to the equilibrium structures of the neutral molecule and the negatively charged ion, respectively. The geometry of each electronic state has been optimized at the CAS-ACPF level of theoretical sophistication. All CAS(2,2)-, CAS(3,2)-, as well as the CAS-ACPF energy calculations and the corresponding geometry optimizations have been performed with the MOLPRO-2000[38] suite of programs.

Since there are no analytical gradients available for the CAS-ACPF approach, all geometry optimizations at this level of theory had to be performed numerically, which has been an enormous challenge concerning computer time. The corresponding numerical calculation of the harmonic vibrational frequencies at this theoretical level would have been absolutely prohibitive; therefore, they have been calculated with the B3LYP hybrid functional, as implemented in the Gaussian 98[39] package in order to assess the zero-point energies (ZPE). For excited negative ion states such as the $^4A''$ states of $HSiNa^-$, $LiSiNa^-$, and $LiSiSiH_3^-$, as well as all dipole-bound negative ion states, for which no ZPE could be calculated at the B3LYP level of theory, the corresponding ZPE of the respective neutral triplet state has been employed. Although this procedure has no serious effect on the calculated EA values, based on past experience, the ZPE corrections employed for the excited negative ion states might be expected to be too large, so the resultant excited states electron affinities should be considered as lower limits for the adiabatic EA values. All isosurface pictures for the dipole-bound SOMOs have been generated with the program MOLDEN.[40]

In a few instances, we have also taken the challenge to investigate the bending potential energy curves to obtain insight into the energetics along the bending motion in a certain electronic state. For this purpose, we have chosen a grid distance of 2° between the calculated points along the angle bending motion within a certain range of angles. At each angle all geometrical variables except the bending angle Φ itself have been optimized at the CAS-ACPF level of theory. So all displayed curves represent CAS-ACPF minimum-energy paths. Such a procedure is tremendously time-consuming, and therefore, we decided to perform it only on two paradigmatic cases (i.e., $HSiSiH_3$ and HSiLi).

II.a Dipole-Bound Negative Ions. Fermi and Teller[41] found that there exists a critical dipole moment $\mu_{\mathrm{crit}} = 1.625$ D within the pure dipole model, such that any system with a permanent dipole moment μ in excess of μ_{crit} can bind an extra electron in its dipole field and give rise to dipole-bound negative ion states.

TABLE 1: Structural Data and Some Dipole Moments and Zero-Point Energies for the Various Electronic States of $HSiSiH_3$ and $HSiSiH_3^-$ and $Si(SiH_3)_2$ and $Si(SiH_3)_2^-$[a]

system	state	method	E (h)	ZPE(h)	R_{HSi}(Å)	R_{SiSi} (Å)	Φ (°)	μ (D)
$HSiSiH_3$	$X\ ^1A'$	B3LYP	−581.376617	0.030189	1.5262	2.4068	88.890	0.262
$HSiSiH_3$	$^3A''$	B3LYP	−581.354490	0.031067	1.4937	2.3377	121.965	0.210
$HSiSiH_3^-$	X^2A''	B3LYP	−581.408399	0.029380	1.5459	2.3877	90.842	
$HSiSiH_3$	X^1A'	CAS(2,2)-ACPF	−580.430223		1.5225	2.3998	89.824	0.250
$HSiSiH_3$	$^3A''$	CAS(2,2)-ACPF	−580.406255		1.4986	2.3920	120.423	0.204
$HSiSiH_3^-$	$X\ ^2A''$	CAS(2,2)-ACPF	−580.487184		1.5439	2.3824	90.733	
$HSiSiH_3^-$	$^2A'$	CAS(2,2)-ACPF	−580.432456		1.4983	2.2801	125.256	
$Si(SiH_3)_2$	$X\ ^1A$	B3LYP	−872.109885	0.048692		2.3932	92.382	0.226
$Si(SiH_3)_2$	$^3B_1$	B3LYP	−870.095588	0.049591		2.3276	126.670	0.094
$Si(SiH_3)_2^-$	$X\ ^2B_1$	B3LYP	−872.137571	0.047805		2.3807	92.795	
$Si(SiH_3)_2$	X^1A	CAS(2,2)-ACPF	−870.636511			2.4257	110.770	0.623
$Si(SiH_3)_2$	$^3B_1$	CAS(2,2)-ACPF	−870.625878			2.3276	141.213	1.245
$Si(SiH_3)_2^-$	X^2B_1	CAS(2,2)-ACPF	−870.722378			2.4179	108.440	
$Si(SiH_3)_2^-$	$^2A_1$	CAS(2,2)-ACPF	−870.674168			2.2848	139.939	

[a] Φ represents the silylene bond angle. All data are obtained with the aug-cc-pVTZ basis set, employing the B3LYP and the CAS(2,2)-ACPF approaches. The zero-point energies, ZPE, have been calculated only at the B3LYP level of theory. For details see the text.

The excess electron in these cases resides in a highly diffuse totally symmetric "orbital'', which is largely located at the positive end of the dipole. Any real molecule, whose other electrons cause additional repulsion with the dipole-bound extra electron, has to have $\mu > \mu_{crit}$ to be able to support a dipole-bound negative ion state to an extent that such a state can be experimentally detected.

Experimental and theoretical experience during the last decades have shown that 2 D $\leq \mu \leq$ 2.5 D is necessary for a real molecule to be able to provide a dipole bound negative ion state. Many research groups have contributed to the understanding of such feebly bound anions. Especially noteworthy are the experimental contributions of the group of Desfrançois and Schermann[42−49] and the theoretical contributions provided by the groups of Jordan,[50−55] Adamowicz,[56−59] and others.[60−69]

Because of the very diffuse structure of the surplus electron in a dipole-bound anion state, these systems cannot be tackled theoretically with standard basis sets, but instead need strong basis set augmentations. Depending on the electron binding energy of the extra electron, the augmentation has to comprise at least highly diffuse s-type and p-type Gaussian functions and sometimes even higher angular momentum basis functions, as has been described by Skurski et al.[70] For this reason, we have decided to place sets of diffuse s-type and diffuse p-type Gaussians at a 4 Å offset from the atom that lies at the positive end of the dipole moment. The exponents α_n of these diffuse Gaussians have been chosen in an even tempered manner, according to

$$\alpha_n = k^n \alpha_0$$

employing $\alpha_0 = 0.02$ and $k = \sqrt{1/10}$ for both the s-type and p-type functions. This leads to 10 even-tempered s-type as well as p-type functions with exponents in the range of 0.02 down to 1×10^{-6}, which seems sufficient for the present purpose, since the electron binding energies for most of the investigated dipole-bound states are in excess of 10 meV. This procedure is very similar to that used by many other groups and practically identical to those made use of in recent studies on dipole-bound anion states of diatomic molecules[71,72] and cyanosilylenes.[30]

III. Results and Discussion

(a) $HSiSiH_3$ and $HSiSiH_3^-$. The essential structural parameters optimized at the B3LYP as well as the CAS-ACPF levels of theory for the investigated electronic states of silylsilylene and its anion are collected in Table 1. It is apparent from inspection of Table 1 that the structural parameters of the B3LYP and the CAS-ACPF optimized structures are highly comparable and moreover these structural characteristics are in good accordance with previous values calculated using pseudopotenitals to describe inner-shell electrons at the CAS(2,2) level of theory.[22] The neutral ground state of $HSiSiH_3$ is the $(\sigma^2\pi^0)$ $^1A'$ state and the lowest excited-state is the $(\sigma^1\pi^1)$ $^3A''$ state. The singlet−triplet gap of 0.676 eV (cf. Table 8) is significantly smaller than in SiH_2. Such a decrease in the singlet−triplet splitting is typical for the silyl substituent. Inspection of Table 8 shows that the first adiabatic electron affinity of silylsilylene is 1.572 eV, which is in good agreement with the correponding BLYP value of 1.56 eV, reported by Larkin et al.[29] Figure 1 displays the bending potential energy curves for the singlet and triplet and anionic states of $HSiSiH_3$ and shows that the $^3A''$ state is favored over the $^1A'$ state for bond angles larger than 125°. It is obvious that the $(\sigma^2\pi^1)$ $^2A''$ negative ion ground state curve is cum grano salis parallel to the $^1A'$ neutral ground state curve, whereas the bending potential energy curve of the $(\sigma^1\pi^2)$ $^2A'$ excited negative ion state runs grossly parallel to that of the $^3A''$ excited neutral state. Not surprisingly, the shapes of the bending curves are determined largely by the occupation of

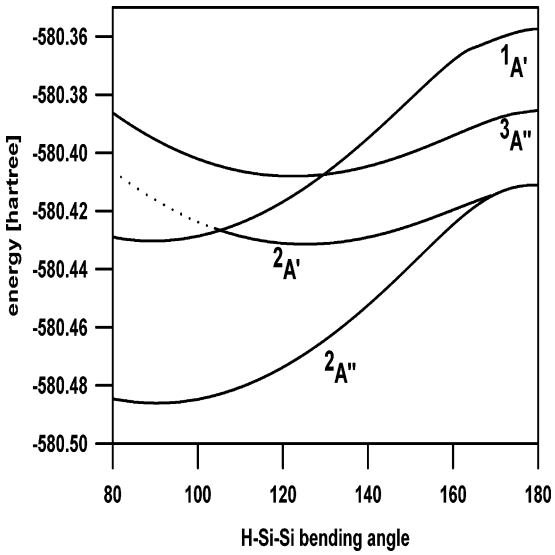

Figure 1. CAS(2,2)-ACPF bending potential energy curves for the X $^1A'$ and $^3A''$ electronic states of $HSiSiH_3$ and the X $^2A''$ and $^2A'$ states of $HSiSiH_3^-$. The calculated points are equidistant with a grid distance of 2°. At each point, all geometry parameters except the silylene bond angle are optimized at the CAS(2,2)-ACPF level.

TABLE 2: Structural Data and Some Dipole Moments and Zero-Point Energies for the Various Electronic States of HSiLi and HSiLi$^-$[a]

system	state	method	$E(h)$	ZPE(h)	R_{XSi} (Å)	R_{SiY} (Å)	Φ (°)	μ (D)
HSiLi(s)	X ^{3}A″	B3LYP	−297.572590	0.006565	1.6106	2.3770	47.668	5.187
HSiLi(l)	^{3}A″	B3LYP	−297.571358	0.006365	1.5080	2.3405	140.329	
HSiLi	^{1}A′	B3LYP	−297.559738	0.006160	1.5384	2.5713	89.155	5.505
HSiLi$^-$ (l)	X ^{2}A″	B3LYP	−297.598875	0.005634	1.5510	2.5409	92.918	
HSiLi$^-$ (s)	^{2}A″	B3LYP	−297.598440	0.005447	1.5893	2.4465	57.246	
HSiLi$^-$ (l)	^{4}A″	B3LYP	−297.598015	0.005675	1.5256	2.4850	151.697	
HSiLi$^-$ (s)	^{4}A″	B3LYP	−297.597288	0.006167	1.5829	2.5998	43.471	
HSiLi(s)	X ^{3}A″	CAS-ACPF	−297.047822		1.6115	2.3994	48.295	6.202
HSiLi(l)	^{3}A″	CAS-ACPF	−297.047227		1.5104	2.3666	139.545	6.680
HSiLi	^{1}A′	CAS-ACPF	−297.035694		1.5402	2.5636	89.644	6.101
HSiLi$^-$ (s)	X ^{2}A″	CAS-ACPF	−297.075622		1.5803	2.5456	55.355	
HSiLi$^-$ (l)	^{2}A″	CAS-ACPF	−297.074649		1.5492	2.6088	95.087	
HSiLi$^-$ (l, d)	^{4}A″	CAS-ACPF	−297.070632		1.5283	2.5223	152.878	
HSiLi$^-$ (s,d)	1^{4}A″	CAS-ACPF	−297.069967		1.5811	2.6301	44.108	
HSiLi$^-$ (s)	^{2}A′	CAS-ACPF	−297.052659		1.6329	2.3714	48.691	
HSiLi$^-$ (l)	^{2}A′	CAS-ACPF	−297.049695		1.5268	2.2968	146.618	
HSiLi$^-$ (l,d)	^{4}A″	CAS-ACPF	−297.047925		(1.5492)	(2.6088)	(95.087)	

[a] All data are obtained with the aug-cc-pVTZ basis set, employing the B3LYP and the CAS-ACPF approaches. The (l) and (s) designators in the first column identify the large- and small-angle conformers and the (d) designator identifies dipole-bound negative ion states. The geometry data in parentheses are not optimized but are adopted from other electronic states, listed in the table. For details see the text.

the σ-orbital. If the H−Si−Si bond angle is linearized (Φ = 180°), both negative ion states coalesce into the ^{2}E state of the $HSiSiH_3^-$ ion in C_{3v} symmetry. The ^{2}E state is not adiabatically stable but exhibits a notable stability with respect to vertical electron detachment. The ^{2}E state of linear (C_{3v}) $HSiSiH_3^-$ lies energetically below any of the neutral states at this nuclear arrangement. Therefore, one could infer that a bound excited negative ion state could also exist. In fact, the adiabatic stability of the ^{2}A′ excited anion state is 0.037 eV. According to our CAS(3,2)-ACPF results, both Jahn−Teller components of the ^{2}E anion state become stabilized upon bending, as can be seen from Figure 1. The equilibrium bond angle of the ^{2}A″ ground state is 90.84°, whereas the equilibrium bond angle of the ^{2}A′ excited negative ion state is 125.26°. The bending potential energy curve of this state crosses that of the ^{1}A′ neutral ground state near 104°. Although the ^{2}A″ anion ground state is stable for all investigated bond angles, the ^{2}A′ excited negative ion state becomes electronically unstable for bond angles near 100° and smaller. This means the ^{2}A′ state is vertically unstable at the ^{1}A′ ground state geometry. The ^{2}A′ excited-state vertical electron detachment energy is calculated as 0.551 eV to arrive at the ^{1}A′ state and 0.665 eV to arrive at the ^{3}A″ state.

(b) $Si(SiH_3)_2$ and $Si(SiH_3)_2^-$. The singlet ground state of $Si(SiH_3)_2$ has C_2 rather than C_{2v} symmetry, since the latter corresponds to a second-order saddle point. The highest-frequency imaginary normal mode with 121*i* cm^{-1} at the C_{2v}-optimized geometry exhibits a_2 symmetry and indicates a distortion to C_2 symmetry, at which the molecule has a positive definite Hessian matrix. The energy gain in going from C_{2v} to C_2 symmetry is not very pronounced but non-negligible and amounts to no more than 0.029 eV. It is interesting to note that the central bond angle Φ for the ^{1}A ground state differs significantly between the B3LYP (92.38°) and the CAS(2,2)-ACPF approach (110.77°). The angular correlation of the σ-type lone-pair described by double excitation into the empty π-type (b_1) orbital, i.e., the $|\cdots(b_1)^2|$ determinant, which enters the CI-vector with a coefficient of −0.22, and which is not present in the DFT ansatz, could account for this difference, since this type of electron correlation would favor a larger bond angle. The lowest triplet state, $(\sigma^1\pi^1)$ ^{3}B$_1$, possesses C_{2v} symmetry. Substituting the silylene-hydrogen of silylsilylene by a second silyl group leads to a further reduction of the singlet−triplet gap to 0.319 eV, as can be seen from Table 8. The $(\sigma^2\pi^1)$ ^{2}B$_1$ negative ion ground state of $Si(SiH_3)_2^-$ binds the extra electron rather strongly, as can be recognized from an adiabatic EA of 2.361 eV. This is significantly larger than the corresponding BLYP-value of 1.95 eV found by Larkin et al.,[29] which is not too much at variance with an older value of 1.70 eV, as calculated by Kalcher and Sax,[22] employing the CAS(2,2)-CI approach and using pseudopotentials for the inner electrons of the Si-atoms. A glance at the EA-values in Table 8 reveals that the second silyl substituent in $Si(SiH_3)_2$ brings about an enormous stabilization of the ^{2}A$_1$ excited negative ion state, which exhibits an EA value of 1.000 eV. This is 0.963 eV larger than the corresponding EA value in silylsilylene. No further stable excited negative ion states could be detected either for $HSiSiH_3^-$ or for $Si(SiH_3)_2^-$.

(c) HSiLi and HSiLi$^-$. Introduction of an Li-substituent into silylene reverses the order of stabilities so the triplets become the neutral electronic ground states. Another new feature is the appearance of two minimum-energy structures on the triplet potential energy hypersurface, which are designated (l) and (s) for the large and small bond angle isomer, respectively. Only the open-shell $(\sigma^1\pi^1)$ triplet states seem to exhibit bond-angle-isomerism, since no such isomers could be found for the $(\sigma^2\pi^0)$ singlet states. It can be seen in Table 2 and in Figure 2 that both ^{3}A″ structures lie energetically below the ^{1}A′ structure and that the small-angle isomer ($\Phi \approx 48°$) ^{3}A″(s) has the lowest energy. The bending potential energy curves displayed in Figure 2 reveal that the barrier between ^{3}A″(s) and ^{3}A″(l) is no larger than 0.2 eV. Finally, the ^{3}A″(s)−^{1}A′ singlet−triplet gap, ΔE_{ST}, is −0.319 eV.

Inspection of Table 8 reveals that silylsilylene and especially disilylsilylene have ground state electron affinities notably in excess of SiH_2, whereas the EA value of 0.772 eV for the X ^{2}A″ negative ion ground state of HSiLi$^-$ is significantly smaller. This is in line with previous findings for the electron affinity of Lithiosilylene.[22] A glance at Figure 2 makes clear that the negative ion ground state cannot really be assigned a unique equilibrium bond angle, since the angle bending potential exhibits only two extremely shallow minima, and the separating barrier is only 0.018 eV. Therefore, one could infer that ^{2}A″ HSiLi$^-$ should undergo large-amplitude angular motions which, in turn, could generate unusual features in, for example, photodetachment spectra.

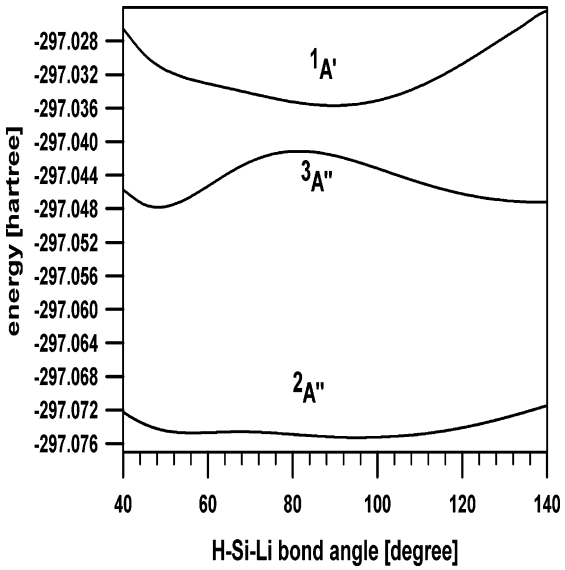

Figure 2. CAS-ACPF bending potential energy curves for the X ^{3}A″ and ^{1}A′ electronic states of HSiLi and the X ^{2}A″ and state of HSiLi$^-$. The calculated points are equidistant with a grid distance of 2°. At each point, all geometry parameters except the silylene bond angle are optimized at the CAS-ACPF level.

It was a big surprise to find that the first excited bound negative ion state of HSiLi$^-$ has $(\sigma^1\pi^1\sigma_{d'}^1)$ ^{4}A″ rather than the expected $(\sigma^1\pi^2)$ ^{2}A′ symmetry. Moreover, there are both large-angle (l) as well as small-angle (s) minima on the ^{4}A″ potential energy hypersurface. The former has the lower energy and leads to an EA value of 0.645 eV, whereas the corresponding EA value for the (s) minimum is 0.613 eV. There is evidence that even a second bound excited $(\sigma^1\pi^1\sigma_d^1)$ $2^4A''$ state exists and unequivocally corresponds to a dipole-bound state with a rather small binding energy of approximately 3 meV (cf. Table 8). The HOMOs, $\sigma_{d'}$ and σ_d, of the 1^4A″ and 2^4A″ states, respectively, deserve some consideration. Despite the fact that the electron binding energy of 1^4A″ is larger than 0.6 eV and can be calculated with the aug-cc-pVTZ basis set, the $\sigma_{d'}$-HOMO, as displayed in Figure 1a, exhibits characteristics of a dipole-bound orbital, since most of the orbital density is found away from the molecule, although it possesses a less inflated structure than most typical dipole-bound orbitals. Consequently, one could address the 1^4A″ state as dipole-bound according to the appearance of the HOMO but not necessarily due to the magnitude of the electron affinity. Jordan[55] has addressed the problems of taxonomy associated with such negative ion states, where the HOMO appears as a dipole-bound orbital, notwithstanding a rather high EA value. No such ambiguities plague us with the $(\sigma^1\pi^1\sigma_d^1)$ 2^4A″ state, which has an EA value in the meV range. The σ_d-HOMO, which is shown in Figure 1b, is also positioned away from the molecule and has a highly inflated appearance, typical for a dipole-bound anion. The $(\sigma^1\pi^2)$ ^{2}A′ excited negative ion state exhibits an adiabatic stability of 0.137 eV, which is four times larger than the EA value of the corresponding state in $HSiSiH_3^-$ and seven times smaller than the EA value calculated for the totally symmetric $^2A_1$ negative ion state in $Si(SiH_3)_2^-$.

(d) HSiNa and HSiNa$^-$. One would expect HSiNa to be similar to HSiLi, since these systems differ only in the alkaline metal substituent. The structural data and the energies listed in Table 3 do not really confirm this expectation in all aspects. As expected, $(\sigma^1\pi^1)$ ^{3}A″ is the neutral ground state potential hypersurface, on which we find two minima, (l) ($\Phi = 131.06°$) and (s) ($\Phi = 54.2°$), but unlike HSiLi, the (l) conformer has the lower energy. The corresponding ΔE_{ST} value amounts to −0.252 eV and is, thus, less negative than in HSiLi. Despite the smaller singlet−triplet gap, the ground state electron affinity for $(\sigma^2\pi^1)$ ^{2}A″ is 0.921 eV, which is 0.15 eV larger than for HSiLi. The EA value for the $(\sigma^1\pi^1\sigma_{d'}^1)$ 1 ^{4}A″ excited negative ion state is 0.756 eV, which is rather close to the ground state EA of HSiLi. The second negative ion state of the same symmetry, $(\sigma^1\pi^1\sigma_d^1)$ 2^4A″, which is a dipole-bound anion state, exhibits a stability of 0.114 eV. The EA-value of the totally symmetric excited anion state, $(\sigma^1\pi^2)^2$A′, is as high as 0.695 eV and, consequently, much higher than the respective value for HSiLi$^-$.

(e) LiSiSiH $_3$ and LiSiSiH$_3^-$. Since a silyl-substituent and even more a lithium-substituent both reduce the singlet−triplet gap in a silylene, it is interesting to explore the combined effect of both substituents in $LiSiSiH_3$. The data presented in Table 4 reveal that LiSiSiH $_3$ possesses, as expected, a $(\sigma^1\pi^1)$ triplet ground state, which has C_1 symmetry, ^{3}A, and which shows a rather large bond angle $\Phi = 152.2°$. The excited $(\sigma^2\pi^0)^1$A state has also C_1 symmetry, but a much smaller equilibrium bond angle $\Phi \approx 82.9°$ at the B3LYP level but a very large bond angle, which exceeds even that of the triplet ground state, at the CAS-ACPF level of theory. Our assumption that there might exist two bond angle isomers, (l) and (s), as for HSiLi could not be substantiated, since even beginning at the B3LYP optimized geometry eventually leads to large-angle structure when further CAS-ACPF optimization is performed (cf. Table 4).

The singlet−triplet gap in $LiSiSiH_3$ is calculated as −0.677, which is the highest negative ΔE_{ST} value of all silylenes

TABLE 3: Structural Data and Some Dipole Moments and Zero-Point Energies for the Various Electronic States of HSiNa and HSiNa$^-$[a]

system	state	method	E (h)	ZPE(h)	R_{XSi}(Å)	R_{SiY} (Å)	Φ (°)	μ (D)
HSiNa	X ^{3}A″	B3LYP	−452.359213	0.005818	1.5199	2.7104	124.359	7.057
HSiNa	^{1}A′	B3LYP	−452.353603	0.005808	1.5379	2.8664	88.172	5.133
HSiNa$^-$	X^{2}A″	B3LYP	−452.398290	0.005192	1.5505	2.8935	91.763	
HSiNa(l)	X ^{3}A″	CAS-ACPF	−451.457766		1.5193	2.7225	131.065	8.493
HSiNa(s)	^{3}A″	CAS-ACPF	−451.456725		1.5923	2.7549	54.190	8.260
HSiNa	^{1}A′	CAS-ACPF	−451.448499		1.5413	2.8898	88.097	6.101
HSiNa$^-$	X ^{2}A′	CAS-ACPF	−451.490971		1.5541	2.9386	89.186	
HSiNa$^-$ (l,d)	$1_{(l)}{}^4$A″	CAS-ACPF	−451.485533		1.5339	2.8809	167.895	
HSiNa$^-$ (l,d)	$2_{(l)}{}^4$A″	CAS-ACPF	−451.461947		(1.5339)	(2.8809)	(167.895)	
HSiNa$^-$ (s,d)	$1_{(s)}{}^4$A″	CAS-ACPF	−451.483965		1.5758	3.0459	47.033	
HSiNa$^-$	^{2}A′	CAS-ACPF	−451.465280		1.6491	3.0476	93.231	

[a] All data are obtained with the aug-cc-pVTZ basis set, employing the B3LYP and the CAS-ACPF approaches. The (l) and (s) designators in the first column identify the large- and small-angle conformers and the (d) designator identifies dipole-bound negative ion states. The geometry data in parentheses are not optimized but are adopted from other electronic states, listed in the table. For details see the text.

TABLE 4: Important Structural Data and Some Dipole Moments and Zero-Point Energies for the Various Electronic States of $LiSiSiH_3$ and $LiSiSiH_3^-$[a]

system	state	method	$E(h)$	ZPE(h)	R_{SiLi} (Å)	R_{SiSi} (Å)	Φ (°)	μ (D)
$LiSiSiH_3$	$X\ ^3A$	B3LYP	−588.312346	0.025435	2.3377	2.3414	152.771	7.272
$LiSiSiH_3$	^1A	B3LYP	−588.299373	0.024625	2.5320	2.3624	82.886	6.173
$LiSiSiH_3^-$	$X\ ^2A''$	B3LYP	−588.350892	0.022443	2.5317	2.3839	99.883	
$LiSiSiH_3$	$X\ ^3A$	CAS(2,2)-ACPF	−587.310747		2.3646	2.3464	152.194	5.883
$LiSiSiH_3$	^1A	CAS(2,2)-ACPF	−587.287953		2.3422	2.3351	176.509	7.810
$LiSiSiH_3^-$	X^2A''	CAS(3,2)-ACPF	−587.345750		2.6172	2.3926	99.826	
$LiSiSiH_3^-$	$^2A'$	CAS(3,2)-ACPF	−587.323539		2.2756	2.3289	158.627	
$LiSiSiH_3^-$ (d)	$1\ ^4A''$	CAS(3,2)-ACPF	−587.340847		(2.3646)	(2.3464)	(152.194)	
$LiSiSiH_3^-$ (d)	$2\ ^4A''$	CAS(3,2)-ACPF	−587.313690		(2.3646)	(2.3464)	(152.194)	

[a] All data are obtained with the aug-cc-pVTZ basis set, employing the B3LYP and the CAS-ACPF approaches. Φ represents the Li−Si−Si angle. The (d) designators in the first column identify the dipole-bound negative ion states. The geometry data in parentheses are not optimized but are adopted from other electronic states, listed in the table. For details see the text.

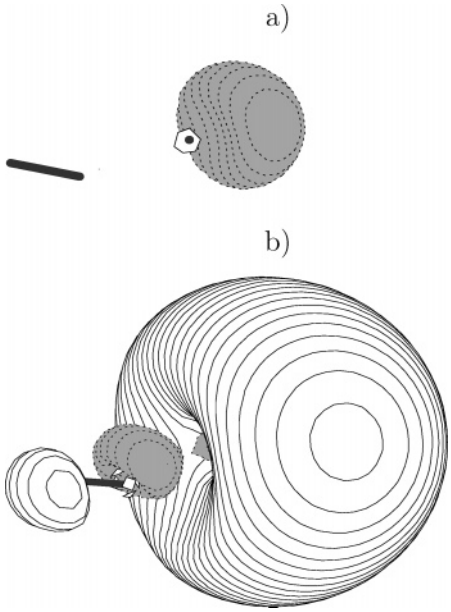

Figure 3. Isocontour plots of the highest SOMO of the $1\ ^4A''$ (a) and the $2\ ^4A''$ (b) excited negative ion states of $HSiLi^-$.

investigated here. Despite the larger negative singlet triplet gap, the ground-state electron affinity of $LiSiSiH_3$ is no more than 0.901 eV (cf. Table 8) and is, thus, only some 0.23 eV larger than for HSiLi. It is interesting to note that the $(\sigma^2\pi^1)$ $X\ ^2A''$ negative ion ground-state has C_s symmetry, although both neutral electronic states exhibit C_1 symmetry. As with $HSiLi^-$, the lowest excited negative ion state in $LiSiSiH_3^-$ is $(\sigma^1\pi^1\sigma_{vd}^1)$ $1^4A''$, which has an EA value of 0.740 eV, some 0.1 eV in excess of the EA value of the corresponding state in $HSiLi^-$. The subscript vd in the σ_{vd} orbital indicates that this orbital represents an unequivocal mixture of a valence- and a dipole-bound orbital, as can be seen in Figure 4a. The second lowest excited-state of $LiSiSiH_3^-$ is $(\sigma^2\pi^0\sigma_d^1)$ $^2A'$ with an electron affinity value of 0.291 eV. Despite this substantial EA value, the contour plot of the SOMO of this state, as displayed in Figure 4b, shows the characteristics of an undisputable dipole-bound negative ion state. The $(\sigma^1\pi^1\sigma_d^1)$ $2^4A''$ state, which is the least stable of the anion states, investigated for $LiSiSiH_3^-$, is also a dipole-bound state.

(f) LiSiNa and $LiSiNa^-$, $SiLi_2$ and $SiLi_2^-$, and $SiNa_2$ and $SiNa_2^-$. The dimetallated silylenes show very similar characteristics, and therefore, they will be discussed together. The mixed metalated silylene, LiSiNa, is found to have two minima on its triplet ground state potential energy hypersurface. The (s) isomer has a bond angle of 69.95°, whereas the energetically lower (l) isomer exhibits a bond angle of 179.1°, which is close

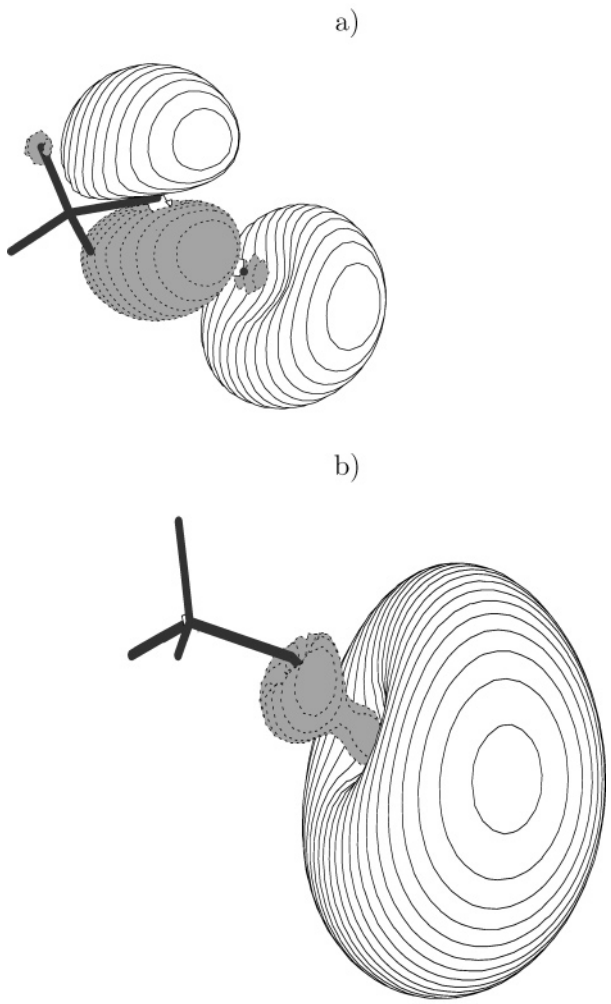

Figure 4. Isocontour plots with a contour value of 0.02 for the highest SOMO of the $1\ ^4A''$ (a) and a contour value of 0.015 for the SOMO of the $^2A'$ (b) excited negative ion states of $LiSiSiH_3^-$.

to linearity (cf. Table 5). This species can be considered as effectively linear (i.e., a $^3\Sigma^-$ state), since the linear conformer lies only 4.05 meV higher in energy than the slightly bent structure at the CAS-ACPF level of theory. This might even be an artifact of our level of calculation because it is known to be very difficult to treat electronic states arising from a $\pi_x^1\,\pi_y^1$ configuration. The ΔE_{ST} gap amounts to −0.377 eV and is somewhat larger than the singlet−triplet splitting in HSiLi. There are a small angle (s) and a large angle (l) conformer on the $(\sigma^2\pi^1)$ $^2A''$ negative ion ground state potential hypersurface and, in contrast to the neutral ground state, the (s) conformer

TABLE 5: Structural Data and Some Dipole Moments and Zero-Point Energies for the Various Electronic States of LiSiNa and $LiSiNa^-$[a]

system	state	method	E (h)	ZPE(h)	R_{SiLi} (Å)	R_{SiNa} (Å)	Φ (°)	μ (D)
LiSiNa(l)	X $^3A''$	B3LYP	−459.291314	0.001734	2.3768	2.7138	179.870	0.255
LiSiNa(s)	$^3A''$	B3LYP	−459.273274	0.002046	2.4500	2.9103	52.052	
LiSiNa	$^1A'$	B3LYP	−459.275311	0.001726	2.5047	2.8192	87.774	5.279
$LiSiNa^-$ (s)	X $^2A''$	B3LYP	−459.318642	0.001537	2.5009	2.8306	83.111	
$LiSiNa^-$ (l)	$^4A''$	B3LYP	−459.312255	0.001497	2.4675	2.8124	179.973	
LiSiNa(l)	X $^3A''$	CAS-ACPF	−458.334904		2.4085	2.7549	179.100	0.500
LiSiNa(s)	$^3A''$	CAS-ACPF	−458.333344		2.5155	2.9251	69.953	5.145
LiSiNa	$^1A'$	CAS-ACPF	−458.321048		2.5209	2.8621	85.429	5.547
$LiSiNa^-$ (s)	X $^2A''$	CAS-ACPF	−458.363517		2.5343	2.8763	79.997	
$LiSiNa^-$ (l)	$^2A''$	CAS-ACPF	−458.354483		2.5561	2.9070	149.179	
$LiSiNa^-$ (d)	$1^4A''$	CAS-ACPF	−458.353586		2.5632	3.1331	63.187	
$LiSiNa^-$ (d)	$2^4A''$	CAS-ACPF	−458.343592		(2.5632)	(3.1331)	(63.187)	
$LiSiNa^-$	$^2A'$	CAS-ACPF	−458.346150		2.4570	2.8824	67.522	

[a] All data are obtained with the aug-cc-pVTZ basis set, employing the B3LYP and the CAS-ACPF approaches. Φ represents the Li−Si−Na angle. The (l) and (s) designators in the first column identify the large- and small-angle conformers and the (d) designator identifies dipole-bound negative ion states. The geometry data in parentheses are not optimized but are adopted from other electronic states, listed in the table. For details see the text.

TABLE 6: Structural Data and Some Dipole Moments and Zero-Point Energies for the Various Electronic States of $SiLi_2$ and $SiLi_2^-$[a]

system	state	method	E (h)	ZPE(h)	R_{SiLi} (Å)	Φ (°)	μ (D)
$SiLi_2$ (l)	X $^3B_1$	B3LYP	−304.502934	0.002266	2.3846	179.872	0.005
$SiLi_2$ (s)	$^3B_1$	B3LYP	−304.492971	0.002175	2.4924	69.740	
$SiLi_2$	X $^1A_1$	B3LYP	−304.482387	0.002193	2.4916	86.439	5.444
$SiLi_2^-$	X $^2B_1$	B3LYP	−304.526816	0.002073	2.4788	78.908	
$SiLi_2^-$	$^2B_2$	B3LYP	−304.511714	0.002308	2.4370	66.949	
$SiLi_2$ (l)	X $^3B_1$	CAS-ACPF	−303.925319		2.4108	178.632	0.157
$SiLi_2$	X $^1A_1$	CAS-ACPF	−303.910317		2.5128	84.454	5.427
$SiLi_2^-$	X $^2B_1$	CAS-ACPF	−303.951571		2.5078	76.037	
$SiLi_2^-$	$^2B_2$	CAS-ACPF	−303.937840		2.4805	66.051	
$SiLi_2^-$ (d)	$^2A_1$	CAS-ACPF	−303.928257		2.3909	152.016	
$SiLi_2^-$	$^4B_1$	CAS-ACPF	−303.945913		2.4903	178.913	

[a] All data are obtained with the aug-cc-pVTZ basis set, employing the B3LYP and the CAS-ACPF approaches. Φ represents the Li−Si−Li angle. The zero-point energies, zpe, have been calculated only at the B3LYP level of theory. The (l) and (s) designators in the first column identify the large- and small-angle conformers and the (d) designator identifies dipole-bound negative ion states. For details see the text.

of $LiSiNa^-$ has the lowest energy. The adiabatic electron affinity results as 0.773 eV, which is almost the same as for HSiLi.

At the B3LYP level of theory, the symmetrically metalated $SiLi_2$ system is found to have an (s) and an (l) conformer, where the latter has the lower energy. Despite an extensive search for the (s) conformer at the CAS-ACPF level of theory, we have been unsuccessful, since any optimization produced the (l) conformer. A crude scan along the bending coordinate of triplet $SiLi_2$ revealed that the energy is monotonically decreasing with increasing Φ until a minimum is reached at the equilibrium value of $\Phi = 178.6°$, which can be seen in Table 6. The singlet−triplet splitting is calculated as −0.406 eV. All relevant calculated electron affinities can be found in Table 8. The ground state electron affinity amounts to 0.720 eV, which is in agreement with the old value of Kalcher and Sax.[22] The first excited negative ion state with an EA value of 0.560 eV is, as expected, the $^4B_1$ state, in conformity with finding the $^4A''$ state as the lowest-lying excited negative ion state for the unsymmetrically metalated silylenes. The wavefunction for the $^4B_1$ state is essentially made up of two CSFs, $\Psi_{^4B_1} = 0.76\Phi_1 + 0.3\Phi_2$, with $\Phi_1 = |\cdots{}^3(\sigma\sigma_{a1})\pi^1\sigma_{b_2}^2\sigma_{b_2*}^0|$, and $\Phi_2 = |\cdots{}^1(\sigma\sigma_{a1})\pi^1\sigma_{b_2}^1\sigma_{b_2*}^1|$, where σ_{a_1} denotes a Li−Li-bonding orbital, and σ_{b_2} and σ_{b_2*} denote the bonding and antibonding b_2 symmetric SiLi orbitals, respectively. From the fact that the sum of squares of these two CI coefficients is smaller than 0.7, it can be inferred that there are various other CSFs with non-negligible contributions to the CI vector. The $(\sigma^1\pi^1\sigma_{a_1}^1)$ $^4B_1$-state of $SiLi_2^-$ has an almost linear geometry, similar to the X $^3A''$ ground state. The second stable excited anion state, which exhibits an electron affinity of 0.340 eV, is the $(\sigma^2\pi^2\sigma_{b_2}^1)$ $^2B_2$ state, which can formally be generated by exciting an electron from the σ_{b_2} orbital to the π orbital in the negative ion ground state. The electron affinity for the $(\sigma^2\pi^0\sigma_d^1)$ $^2A_1$ state is 0.080 eV, which is 1 order of magnitude smaller than the corresponding value for $Si(SiH_3)_2^-$. Despite the fact that this EA-value is in excess of that for the $^2A'$ state of $HSiSiH_3^-$, the latter corresponds to a valence-bound excited negative ion state, whereas Figure 5 demonstrates the dipole-bound nature of the $(\sigma^2\pi^0\sigma_d^1)$ $^2A_1$ state of $SiLi_2^-$.

Table 7 shows that the characteristics of the electronic state of $SiNa_2$ as well as those of the anion resemble rather closely those of $SiLi_2$ and its anion. The ΔE_{ST} value of −0.347 is somewhat more positive than for $SiLi_2$. The ground state EA of 0.868 eV for the $(\sigma^2\pi^1)$ $^2B_1$ negative ion ground state is almost 0.15 eV larger than that of $SiLi_2$. The EA values of the first and second excited anion states of $SiNa_2^-$ differ by no more than −0.046 and −0.076 eV, respectively, from the corresponding EA values of $SiLi_2^-$, as can be seen from Table 8. Similar to $SiLi_2^-$, the $(\sigma^1\pi^1\sigma_{a_1}^1)$ $^4B_1$ state is the lowest excited negative ion state of $SiNa_2^-$. The orbital occupation is very similar to that in $SiLi_2^-$ ($^4B_1$), mentioned above. The only difference is that the wavefunction of $SiNa_2^-$ ($^4B_1$) is made up of two almost equally weighted configurations, i.e., $\Psi_{^4B_1} = 0.6\Phi_1 + 0.54\Phi_2 + \cdots$, with various contributions from further CSFs. Figure 6 exhibits that, akin to $SiLi_2^-$, the $(\sigma^2\pi^0\sigma_d^1)$ $^2A_1$ excited-state of $SiNa_2^-$ is also a dipole-bound state. Small remnants from the valence orbitals are still visible in the

TABLE 7: Structural Data and Some Dipole Moments and Zero-Point Energies for the Various Electronic States of $SiNa_2$ and $SiNa_2^-$[a]

system	state	method	E (h)	ZPE(h)	R_{SiNa} (Å)	Φ (°)	μ (D)
$SiNa_2$	$X\ ^3B_1$	B3LYP	−614.0799866	0.001213	2.7108	169.290	
$SiNa_2$	$^1A_1$	B3LYP	−614.066217	0.001248	2.8286	90.320	
$SiNa_2^-$	X^2B_1	B3LYP	−614.111439	0.001061	2.8511	88.188	
$SiNa_2$	X^3B_1	CAS-ACPF	−612.744595		2.7528	178.699	0.117
$SiNa_2$	$^1A_1$	CAS-ACPF	−612.731842		2.8696	86.937	5.517
$SiNa_2^-$	$X\ ^2B_1$	CAS-ACPF	−612.776354		2.9013	84.247	
$SiNa_2^-$	$^2B_2$	CAS-ACPF	−612.754147		2.8615	69.322	
$SiNa_2^-$ (d)	$^2A_1$	CAS-ACPF	−612.747711		2.9548	76.549	
$SiNa_2^-$	$^4B_1$	CAS-ACPF	−612.763491		2.9603	90.345	

[a] All data are obtained with the aug-cc-pVTZ basis set, employing the B3LYP and the CAS-ACPF approaches. Φ represents the Li−Si−Li angle. The zero-point energies, ZPE, have been calculated only at the B3LYP level of theory. The (l) and (s) designators in the first column identify the large- and small-angle conformers and the (d) designator identifies dipole-bound negative ion states. For details see the text.

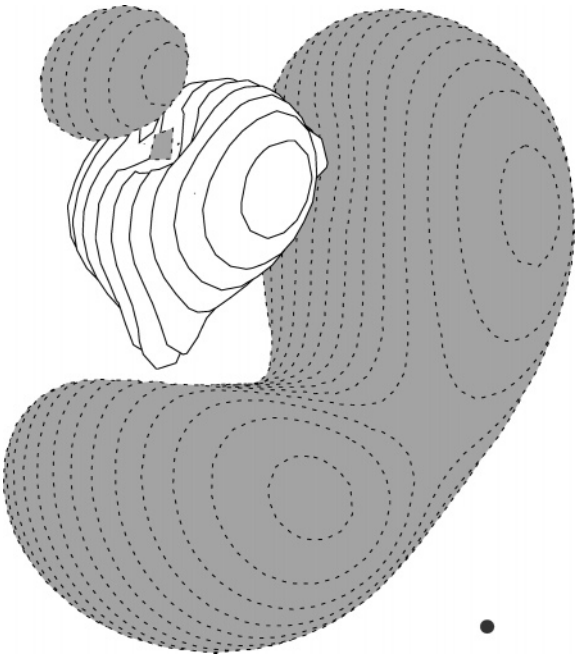

Figure 5. Isocontour plot with a contour value of 0.015 for the SOMO of the $^2A_1$ excited negative ion state of $SiLi_2^-$.

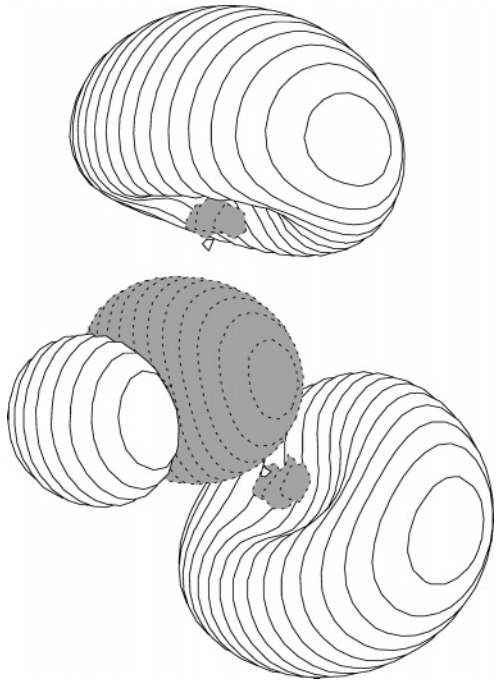

Figure 6. Isocontour plot with a contour value of 0.015 for the SOMO of the $^2A_1$ excited negative ion state of $SiNa_2^-$.

TABLE 8: Singlet−Triplet Splittings, ΔE_{ST}, and EA Values for the Investigated Silylenes[a]

system	ΔE_{ST}	electron affinities (EA)
$HSiSiH_3$	0.676	1.572 (X^2A''), 0.037 ($^2A'$)
$Si(SiH_3)_2$	0.319	2.361 (X^2B_1), 1.000 ($^2A_1$)
HSiLi	−0.319	0.772 (X^2A''), 0.645 ($1^4A''$), 0.137 ($^2A'$), 0.003 ($2^4A''$)
HSiNa	−0.252	0.921 (X^2A''), 0.756 ($1^4A''$), 0.695 ($^2A'$), 0.114 ($2^4A''$)
$LiSiSiH_3$	−0.677	0.901 (X^2A''), 0.740 ($1^4A''$), 0.291 ($^2A'$), 0.023 ($2^4A''$)
NaSiLi	−0.377	0.773 (X^2A''), 0.508 ($1^4A''$), 0.306 ($^2A'$), 0.236 ($2^4A''$)
$SiLi_2$	−0.406	0.720 (X^2B_1), 0.560 (1^4B_1), 0.340 ($^2B_2$), 0.080 ($^2A_1$)
$SiNa_2$	−0.347	0.868 (X^2B_1), 0.514 (1^4B_1), 0.264 ($^2B_2$), 0.084 ($^2A_1$)

[a] All values are given in eV. The negative ion state to which the corresponding EA value refers is given in parentheses.

isocontour display. The electron affinity of 0.084 eV for this state is highly comparable to that of $SiLi_2^-$ ($^2A_1$).

IV. Conclusions

The reported ΔE_{ST} values of SiH_2, as determined experimentally by Kasdan et al.[21] and Berkowitz et al.[73] and theoretically by Balasubramanian and McLean,[74] are close to 21 kcal/mol ≅ 0.91 eV. The experimentally as well as theoretically accepted ground state EA value for silylene, as cited by Damrauer and Hankin[24] is 1.124 ± 0.03 eV. Our CAS-ACPF calculations show that a silyl-substituent reduces the singlet−triplet splitting of a silylene, in comparison to the unsubstituted SiH_2 system, resulting in ΔE_{ST} values of 0.676 and 0.319 eV for $HSiSiH_3$ and $Si(SiH_3)_2$, respectively. The corresponding ground state electron affinities, referring to the $^2A''$ and the $^2B_1$ anion ground states, are 1.572 and 2.361 eV, respectively. These EA values are significantly larger than the electron affinity of SiH_2. Moreover, silylsilylene and disilylsilylene both possess totally symmetric bound excited negative ion states with corresponding EA values of 0.037 and 1.000 eV.

The electropositive akaline metal substituents lead to negative singlet−triplet splittings; that is, the neutral ground states have triplet multiplicity and also give rise to bond angle isomerism, in that several species possess structures with a large and a small bond angle in their triplet neutral ground states as well in several negatively charged electronic states. HSiLi has been found to have $\Delta E_{ST} = -0.319$ eV. Interestingly, the introduction of a second Li-substituent leads only to a marginal effect of approximately −0.1 eV on the ΔE_{ST} values, yielding a singlet−triplet splitting of no more than −0.406 eV for $SiLi_2$. A sodium-

substituent has significantly less efficiency than Li in reducing ΔE_{ST} values, so that HSiNa exhibits a singlet−triplet splitting of −0.252 eV, which is the least negative of all investigated metalated silylenes. The following sequence of energetic separations between the neutral singlet and triplet states can thus be derived

$$HSiSiH_3 > Si(SiH_3)_2 > 0 > HSiNa > HSiLi > SiNa_2 > NaSiLi > SiLi_2 > LiSiSiH_3$$

There is, however, no such clear-cut trend for the ground state EAs. For positive ΔE_{ST} values, we could infer that the EAs become larger with smaller singlet−triplet splittings. However, the two points on which this supposition is based do not allow us to make a conclusive statement about whether or not there is a functional dependence of the EA values on the ΔE_{ST} values. The series of ground state EAs for the $(\sigma^2\pi^1)$ anion ground states reads as follows

$$Si(SiH_3)_2 > HSiSiH_3 > 1eV > HSiNa > LiSiSiH_3 > SiNa_2 > NaSiLi \approx HSiLi > SiLi_2$$

The most stable excited negative ion state with an EA value of 1.000 eV is found to be the $(\sigma^1\pi^2)$ $^2A_1$ state of $Si(SiH_3)_2^-$, whereas the comparable $(\sigma^1\pi^2)$ $^2A'$excited-state of $HSiSiH_3^-$ has only a very small stability of 0.037 eV. The ground state EAs of the metalated silylenes are found between 0.72 and 0.92 eV. Interestingly, the first excited anion state are the $(\sigma^1\pi^1\sigma_{d'}^1)$ $1^4A''$ states for the unsymmetrically substituted species. The $\sigma_{d'}$ orbitals denote dipole-bound orbitals, with various degrees of valence-type contributions. The lowest excited negative ion states for the symmetrically dimetallated species SiX_2^- are the $(\sigma^1\sigma_{a_1}^1\pi^1)$ $^4B_1$ states. The σ_{a1} represents a bonding orbital of the X_2 moiety. The EA values of these first excited negative ion states lie between 0.508 and 0.756 eV. The second excited negative ion states are the $(\sigma^1\pi^2)$ $^2A'$ states of $HSiLi^-$, $LiSiSiH_3^-$, $NaSiLi^-$, and $HSiNa^-$. The corresponding excited negative ion states of $SiLi_2^-$ and $SiNa_2^-$ are the $(\sigma^2\pi^2\sigma_{b_2})$ $^2B_2$ states, which can be produced formally by lifting one electron of the doubly occupied b_2 orbital in the negative ion ground state to the singly occupied π orbital. The pertinent electron affinities range from 0.137 to 0.695 eV. The third excited anion states of $HSili^-$, $LiSiSiH_3^-$, $NaSiLi^-$, and $HSiNa^-$ are the $(\sigma^1\pi^1\sigma_d^1)$ 2 $^4A''$ states, while the third excited negative ion states of $SiLi_2^-$ and $SiNa_2^-$ are $(\sigma^2\sigma_d^1)$ $^2A_1$states. All of these third excited states have the characteristics of dipole-bound anion states.

Acknowledgment. This work was supported in part by NSF Grant CHE-0240387.

References and Notes

(1) Pause, L.; Robert, M.; Heinicke, J.; Kuhl, O. *J. Chem. Soc., Perkin Trans. 2* **2001**, 1383.
(2) Bhandarkar, U. V.; Swihart, M. T.; Girshick, S. L.; Kortshagen, U. R. *J. Phys. D* **2000**, *33*, 2731.
(3) West, R.; Moser, D. F.; Haaf, M.; Schmedake, T.; Guzei, I. In *Organosilicon Chemistry V*; Auner, N, Weis, J., Eds.; John Wiley and Sons: New York, 2003.
(4) Mavridis, A.; Harrison, J. F. *Acc. Chem. Res.* **1974**, *7*, 378.
(5) Harrison, J. F.; Liedtke, R. C.; Liebman, J. F. *J. Am. Chem. Soc.* **1979**, *101*, 7162.
(6) Mueller, P. H.; Rondan, N. G.; Houk, K. N.; Harrison, J. F.; Hooper, D.; Willen, B. H.; Liebman, J. F. *J. Am. Chem. Soc.* **1981**, *103*, 5049.
(7) Mavridis, A.; Harrison, J. F. *J. Am. Chem. Soc.* **1982**, *104*, 3827.
(8) Mavridis, A.; Harrison, J. F. *J. Phys. Chem.* **1982**, *86*, 1979.
(9) Apeloig, Z.; Pauncz, R.; Karni, M.; West, R.; Steiner, W.; Chapman, D. *Organometallics* **2003**, *22*, 3250.
(10) Gordon, M. S. *Chem. Phys. Lett.* **1985**, *114*, 348.
(11) Gaspar, P. P.; Xiao, M.; Pae, D. H.; Berger, D. J.; Haile, T.; Chen, T.; Lei, D.; Winchester, W. R.; Jiang, P. *J. Organomet. Chem.* **2002**, *646*, 68.
(12) Slipchenko, L. V.; Krylov, A. I. *J. Chem. Phys.* **2002**, *117*, 4694.
(13) Weidenbruch, M. *J. Organomet. Chem.* **2002**, *646*, 39.
(14) Yoshida, M.; Tamaoki, N. *Organometallics* **2002**, *21*, 2587.
(15) Sekiguchi, A.; Tanaka, T.; Ichinohe, M.; Akiyama, K.; Tero-Kubota, S. *J. Am. Chem. Soc.* **2003**, *125*, 4962.
(16) Colvin, M. E.; Breulet, J.; Schaefer, H. F., III. *Tetrahed.* **1985**, *41*, 1429.
(17) Boldyrev, A. I.; Simons, J.; v. R. Schleyer, P. *J. Chem. Phys.* **1993**, *99*, 8793.
(18) Boldyrev, A. I.; Simons, J. *J. Phys. Chem.* **1993**, *97*, 1526.
(19) Boldyrev, A. I.; Simons, J. *J. Phys. Chem.* **1993**, *97*, 6149.
(20) Grev, R. S.; Schaefer, H. F., III.; Gaspar, P. P. *J. Am. Chem. Soc.* **1991**, *113*, 5638.
(21) Kasdan, A.; Herbst, E.; Lineberger, W. C. *J. Chem. Phys.* **1975**, *62*, 542.
(22) Kalcher, J.; Sax, A. F. *J. Mol. Struct. (THEOCHEM)* **1992**, *253*, 287.
(23) Kalcher, J.; Sax, A. F. *Chem. Rev.* **1994**, *94*, 2291.
(24) Damrauer, R.; Hankin, J. A. *Chem. Rev.* **1995**, *95*, 1137.
(25) King, R. A.; Mastryukov, V. S.; Schaefer, H. F., III. *J. Chem. Phys.* **1996**, *105*, 6880.
(26) Swihart, M. T. *J. Phys. Chem. A* **2000**, *104*, 6083.
(27) Kalcher, J.; Sax, A. F. *Recent Res. Devel. Phys. Chem.* **2000**, *4*, 1.
(28) Rienstra-Kiracofe, J. C.; Tschumper, G. S.; Schaefer, H. F., III.; Nandi, S.; Ellison, G. B. *Chem. Rev.* **2002**, *102*, 231.
(29) Larkin, J. D.; Schaefer, H. F., III. *J. Chem. Phys.* **2004**, *121*, 9361.
(30) Kalcher, J. *J. Phys. Chem. A* **2005**, *109*, 11437.
(31) Gnaser, H. *Phys. Rev. A* **1999**, *60*, R2645.
(32) Dreuw, A.; Sommerfeld, T.; Cederbaum, L. S. *Theor. Chem. Acc.* **1998**, *100*, 60.
(33) Dreuw, A.; Cederbaum, L. S. *Phys. Rev. A* **1999**, *59*, 2702.
(34) Dunning, T. *J. Chem. Phys.* **1989**, *90*, 1007.
(35) Woon, D. E.; Dunning, T. *J. Chem. Phys.* **1993**, *98*, 1358.
(36) Werner, H.-J.; Knowles, P. J. *Chem. Phys. Lett.* **1985**, *115*, 259.
(37) Gdanitz, R. J.; Ahlrichs, R. *Chem. Phys. Lett.* **1988**, *143*, 413.
(38) MOLPRO is a package of ab initio programs written by H.-J. Werner and P. J. Knowles, with contributions from Amos, R. D., Berning, A., Cooper, D. L., Deegan, M. J. O., Dobbyn, A. J., Eckert, F., Hampel, C., Hetzer, G., Leininger, T., Lindh, R., Lloyd, A. W., Meyer, W., Mura, M. E., Nickla*β*, A., Palmieri, P., Peterson, K., Pitzer, R., Pulay, P., Rauhut, G., Schütz, M., Stoll, H., Stone, A. J., Thorsteinsson, T.
(39) Frisch, M. J.; Trucks, G. W.; Schlegel, H. B.; Scuseria, G. E.; Robb, M. A.; Cheeseman, J. R.; Zakrzewski, V. G.; Montgomery, J. A., Jr.; Stratmann, R. E.; Burant, J. C.; Dapprich, S.; Millam, J. M.; Daniels, A. D.; Kudin, K. N.; Strain, M. C.; Farkas, O.; Tomasi, J.; Barone, V.; Cossi, M.; Cammi, R.; Mennucci, B.; Pomelli, C.; Adamo, C.; Clifford, S.; Ochterski, J.; Petersson, G. A.; Ayala, P. Y.; Cui, Q.; Morokuma, K.; Malick, D. K.; Rabuck, A. D.; Raghavachari, K.; Foresman, J. B.; Cioslowski, J.; Ortiz, J. V.; Stefanov, B. B.; Liu, G.; Liashenko, A.; Piskorz, P.; Komaromi, I.; Gomperts, R.; Martin, R. L.; Fox, D. J.; Keith, T.; Al-Laham, M. A.; Peng, C. Y.; Nanayakkara, A.; Gonzalez, C.; Challacombe, M.; Gill, P. M. W.; Johnson, B. G.; Chen, W.; Wong, M. W.; Andres, J. L.; Head-Gordon, M.; Replogle, E. S.; Pople, J. A. *Gaussian 98*, revision 7; Gaussian, Inc.: Pittsburgh, PA, 1998.
(40) Schaftenaar, G.; Noordik, J. H. *J. Comput.-Aided Mol. Des.* **2000**, *14*, 123.
(41) Fermi, E.; Teller, E. *Phys. Rev.* **1947**, *72*, 399.
(42) Desfrançois, C.; Abdoul-Carime, H.; Khelifa, N.; Schermann, J. P. *Phys. Rev. Lett.* **1994**, *73*, 2436.
(43) Abdoul-Carime, H.; Desfrançois, C. *Eur. Phys. J. D* **1998**, *2*, 149.
(44) Desfrançois, C.; Abdoul-Carime, H.; Schermann, J.-P. *Int. J. Mod. Phys. B* **1996**, *10*, 1339.
(45) Desfrançois, C.; Abdoul-Carime, H.; Schermann, J. P. *J. Chem. Phys.* **1996**, *104*, 7792.
(46) Desfrançois, C.; Periquet, V.; Bouteille, Y.; Schermann, J. P. *J. Phys. Chem. A* **1998**, *102*, 1274.
(47) Desfrançois, C.; Abdoul-Carime, H.; Carles, S.; Périquet, V.; Schermann, J. P.; Smith, D. A. M.; Adamowicz, L. *J. Chem. Phys.* **1999**, *110*, 11876.
(48) Lecomte, F.; Schermann, J. P.; Desfrançois, C. In *Prospect of Negative Ions*; Kalcher, J., Ed.; Research SignPost: Trivandrum, 2002; p 29.
(49) Lecomte, F.; Lucas, B.; Grégoire, G.; Schermann, J. P.; Desfrançois, C. *Phys. Chem. Chem. Phys.* **2003**, *5*, 3320.
(50) Jordan, K. D.; Wang, F. *J. Chem. Phys.* **1976**, *64*, 2760.
(51) Jordan, K. D.; Wendoloski, J. *Chem. Phys.* **1977**, *21*, 145.
(52) Jordan, K. D.; Wendoloski, J. *Mol. Phys.* **1978**, *35*, 223.

(53) Jordan, K. D. *Acc. Chem. Res.* **1979**, *12*, 36.
(54) Gutowski, M.; Skurski, P.; Boldyrev, A. I.; Simons, J.; Jordan, K. D. *Phys. Rev. A* **1996**, *54*, 1906.
(55) Jordan, K. D.; Wang, F. *Annu. Rev. Phys. Chem.* **2003**, *54*, 367.
(56) Smets, J.; Smith, D. M. A.; Elkadi, Y.; Adamowicz, L. *J. Phys. Chem. A* **1997**, *101*, 9157.
(57) Smith, D. M. A.; Smets, J.; Elkadi, Y.; Adamowicz, L. *Chem. Phys. Lett.* **1999**, *305*, 169.
(58) Smith, D. A. M.; Jalbout, A. F.; Smets, J.; Adamowicz, L. *Chem. Phys.* **2000**, *260*, 45.
(59) Smith, D.; Adamowicz, L. In *Prospect of Negative Ions*; Kalcher, J., Ed.; Research SignPost: Trivandrum, 2002; p 139.
(60) Gutowski, M.; Skurski, P. *Chem. Phys. Lett.* **1999**, *303*, 65.
(61) Gutowski, M.; Skurski, P.; Simons, J. *Int. J. Mass. Spectrom.* **2000**, *201*, 245.
(62) Gutowski, M.; Skurski, P.; Li, X.; Wang, L.-S. *Phys. Rev. Lett.* **2000**, *85*, 3145.
(63) Skurski, P.; Gutowski, M.; Simons, J. *J. Chem. Phys.* **1999**, *110*, 274.
(64) Skurski, P.; Gutowski, M.; Simons, J. *J. Chem. Phys.* **1999**, *111*, 9469.
(65) Skurski, P.; Gutowski, M.; Simons, J. *Chem. Phys. Lett.* **2000**, *322*, 175.
(66) Skurski, P.; Simons, J. *J. Chem. Phys.* **2000**, *112*, 6563.
(67) Skurski, P.; Rak, J.; Simons, J.; Gutowski, M. *J. Am. Chem. Soc.* **2001**, *123*, 11073.
(68) Wang, X.-B.; Ding, C.-F.; Wang, L.-S.; Boldyrev, A. I.; Simons, J. *J. Chem. Phys.* **1999**, *110*, 4763.
(69) Simons, J.; Skurski, P. In *Prospect of Negative Ions*; Kalcher, J., Ed.; Research SignPost: Trivandrum, 2002; p 117.
(70) Skurski, P.; Gutowski, M.; Simons, J. *Int. J. Quantum Chem.* **2000**, *76*, 197.
(71) Kalcher, J.; Sax, A. F. *J. Mol. Struct. (THEOCHEM)* **2000**, *498*, 77.
(72) Kalcher, J.; Sax, A. F. *Chem. Phys. Lett.* **2000**, *326*, 80.
(73) Berkowitz, J. L.; Green, J. P.; Cho, H.; Ruscic, R. *J. Chem. Phys.***1987**, *86*, 1235.
(74) Balasubramanian, K.; McLean, A. D. *J. Chem. Phys.* **1986**, *85*, 5117.